Desalination 452 (2019) 17–28

Contents lists available at ScienceDirect

Desalination

journal homepage: www.elsevier.com/locate/desal

Synthesis of polybenzimidazole (PBI) forward osmosis (FO) membrane and computational fluid dynamics (CFD) modeling of concentration gradient across membrane surface

Nawshad Akther[a], Sahar Daer[a], Qiang Wei[b], Isam Janajreh[c], Shadi W. Hasan[a,*]

[a] Center for Membrane and Advanced Water Technology, Department of Chemical Engineering, Khalifa University of Science and Technology, Masdar City Campus, P.O. Box 127788, Abu Dhabi, UAE
[b] Trevi Systems Inc., 1415 N McDowell Blvd A, Petaluma, CA 94954, USA
[c] Department of Mechanical Engineering, Khalifa University of Science and Technology, Masdar City Campus, P.O. Box 127788, Abu Dhabi, UAE

ARTICLE INFO

Keywords:
Polybenzimidazole
Forward osmosis membrane
Desalination
Cell orientation
Computational fluid dynamics

ABSTRACT

This research study aimed to synthesize polybenzimidazole (PBI) FO flat sheet membranes for seawater desalination in high temperature and salinity regions like the UAE. The fabrication conditions that were considered to improve membrane performance included casting thickness, oven temperature and duration. The impact of draw and feed solution flow rates, draw solution type and concentration was also investigated. The ideal fabrication conditions for 15 wt% PBI FO membranes were found to be 150 μm casting thickness, heat treatment for 1.5 min at 165 °C and an immersion duration of 10 min in coagulation bath at 23 °C. Performance results showed that the optimal membrane achieved a water flux and salt rejection of 4.2 LMH and 97.4%, respectively with 2 M $MgCl_2$ draw solution, which increased 21.3 LMH and 98.8%, respectively when the draw solution was allowed to flow in the top compartment of the membrane cell (orientation B). Additionally, computational fluid dynamics (CFD) modeling was used to study the impact of concentration gradient across membrane film on water flux and salt rejection at different FO cell orientation when operated at low cross-flow velocities. CFD modeling results demonstrated that solution density, gravity and diffusion rate affected FO performance at low cross-flow velocity.

1. Introduction

There is an urgent need to look for sustainable energy-efficient solutions to seawater desalination, mainly due to the stress of the world energy crisis. Large-scale deployments for seawater desalination using forward osmosis (FO) process can be promising in terms of energy savings as they are osmotically-driven and require low hydraulic pressure. FO is a developing membrane separation process that uses a semi-permeable membrane and is driven by the osmotic pressure gradient existing between a high concentrated solution (draw) and a relatively low concentrated solution (feed) [1,2]. FO can be used for many applications like desalination [3,4], product concentration (food processing), wastewater concentration, power generation [5–7], and treatment of complex effluents from landfill, industry, etc. [8–12]. Additionally, FO processes have several advantages like low fouling propensity of FO membranes, lower operating pressure than reverse osmosis (RO) systems, and elimination of a wide range of ion contaminants [13]. Moreover, membrane fouling in FO can be removed easily by physical cleaning with minimal requirement for chemical cleaning agents [8,14]. Compared to other pressure-driven membrane processes, greater water recovery can be achieved using FO [15]. However, FO can only help in lowering the operating costs if highly efficient FO membranes, suitable draw solutions, and their regeneration methods can be established both technically and economically [16]. Poor membrane performance and highly energy-intensive draw solution regeneration step in FO prevent it from becoming economically viable [17–20]. The commercially available FO membranes like cellulose triacetate (CTA) are unable to perform well at high temperatures and salinities, and they biodegrade readily. Hence, are not suitable for FO seawater desalination in the high-temperature regions like the Middle East. Therefore, it is necessary to develop selective and permeable membranes that can operate well at temperatures of 40 °C or higher [5,21].

To address these issues, polybenzimidazole (PBI) can be used for preparing thermally and chemically stable FO flat-sheet membranes. PBI is a class of aromatic heterocyclic-based polymers, which was

* Corresponding author.
E-mail address: shadi.hasan@ku.ac.ae (S.W. Hasan).

https://doi.org/10.1016/j.desal.2018.11.003
Received 23 June 2018; Received in revised form 9 November 2018; Accepted 20 November 2018
Available online 16 November 2018
0011-9164/

commercially developed in 1983 by the Celanese Corporation [22]. It has robust mechanical strength, remarkable chemical and thermal stability, and does not ignite easily. Hence, PBI membranes were studied for application in membrane processes like nanofiltration (NF), RO, and as ion-exchange membranes in fuel cells [23–28]. PBI membranes were also used for hydrogen carbon dioxide separation [29], heavy metals removal from wastewater [30] and osmotic power generation [31] among other applications. PBI becomes self-charged in the aqueous environment because the adjacent benzene ring delocalizes the imidazole group's proton [32], which makes it suitable for application in water separation process. Wang et al. developed PBI nanofiltration hollow fiber FO membrane and reported that PBI membranes could produce high water flux in FO processes [33,34]. However, salt rejection and hydrophilicity of virgin PBI membrane were found to be comparatively low.

Several researchers have tried to overcome the drawbacks of PBI membranes by modifying their surface and enhancing their properties. Wang et al. successfully modified NF PBI hollow fiber membrane (HFM) with p-xylene to reduce the pore size in the membrane's active layer to a molecular level [35]. Whereas, other researchers functionalized PBI membranes to improve their hydrophilicity and impart surface charge [36,37]. The high chemical, thermal and mechanical stability of PBI membranes will likely increase their shelf life and reduce their maintenance cost; thereby, making PBI an attractive choice for membrane fabrication.

Therefore, the aim of this work was to synthesize and characterize asymmetric PBI FO flat sheet membranes for seawater desalination in high temperature and high salinity regions. The PBI membranes were prepared using the immersion phase inversion technique, and their performance was tested using a bench-scale FO testing unit. The effect of following membrane fabrication parameters on membrane performance was studied: (1) casting thickness (2) oven temperature and (3) duration of polymer solution film in the oven. Additionally, computational fluid dynamics (CFD) modeling was used to study the impact of concentration gradient across membrane film on water flux and salt rejection at different FO cell orientations. Table 1 presents the objectives of the current and previous studies on PBI FO membranes indicating the contribution of this study to the current field of knowledge.

2. Experimental

2.1. Materials

PBI dope for membrane preparation was provided by PBI Performance Products, Inc. (Charlotte, NC) as a 26 wt% solution comprising of 1.5 wt% LiCl and 72.5 wt% dimethylacetamide (DMAc). Glycerol (> 99%) was supplied by Fisher Scientific, USA. Deionized (DI) water (Millipore) was used as feed solution. Three reagent grade inorganic salts were used to prepare draw solutions: sodium chloride (NaCl, 100%, VWR BDH Prolabo®, Belgium), magnesium chloride ($MgCl_2$, > 99%, SDFCL, India) and potassium bromide (KBr, > 99%, Scott Science, England).

2.2. PBI flat sheet membrane fabrication

All PBI flat sheet membranes were prepared in-house. The PBI dope dilution and membrane preparation procedure is described elsewhere [25]. Briefly, the desired PBI dope concentration of 15 wt% was obtained by diluting the 26 wt% PBI dope with DMAc, while maintaining the benzyl alcohol concentration at 28.6 wt%. The PBI dope mixture was stirred at 40 °C for 24 h to obtain a homogenous dope solution, which was left to degas at room temperature for 24 h.

The dope solution was then cast on a woven polyester fabric taped to a clean glass plate using an automatic thin film coater and a casting knife to form a uniform film of desired thickness. The glass plate with the cast film was then placed in an oven at a preset temperature for the desired duration. The cast film was then immersed immediately for 10 min into a coagulant bath containing water at room temperature for phase-inversion to take place. The prepared membrane was then rinsed with DI water and stored in 30% (v/v) aqueous solution of glycerol containing sodium metabisulfite to prevent membrane damage and fouling during storage. The membrane fabrication conditions that were considered during phase inversion method were membrane casting thickness (100, 150 and 200 μm), oven temperature (100 and 165 °C) and heat treatment duration (10, 20 and 30 min).

2.3. Membrane characterization

The mechanical properties of PBI flat sheet FO membranes were investigated using Instron 5966 Dual Column Testing System (Italy).

Table 1
Previous studies on PBI FO membranes and their objectives.

Type of PBI FO membrane	Novelty/Objectives	Year & reference
PBI flat-sheet membrane	Optimization of PBI flat-sheet membrane fabrication conditions. Using CFD modeling to verify the impact of concentration gradient across membrane film on water flux and salt rejection.	This work
PBI NF hollow fiber (HF) membrane	Investigating the feasibility of using PBI NF HF membrane for FO processes.	2007 [33]
PBI NF HF membrane with a thin wall	Chemically modifying PBI NF HF membranes via p-xylylene dichloride cross-linking to tune the mean pore size and improve salt selectivity for application in FO seawater desalination.	2009 [38]
Dual-layer PBI-polyethersulfone (PES) NF HF membrane	Developing dual-layer PBI-PES NF HF membrane with an ultrathin selective skin for water production in FO process.	2009 [39]
Dual-layer PBI-polyethersulfone (PES)/polyvinyl pyrrolidone (PVP) NF HF membrane	Fabricating and applying dual-layer PBI–PES/PVP NF HF membranes in FO process for the protein concentration and enrichment from pharmaceutical products.	2009 [40]
Cellulose acetate (CA) NF HF membranes	Developing and investigating the potential of CA NF HF membranes for FO applications.	2010 [41]
Dual-layer HF membrane with a polyacrylonitrile (PAN)/ PVP inner layer and PBI/ polyhedral oligomeric silsesquioxane (POSS) outer layer	Synthesis of a mixed matrix dual-layer HF membrane comprising of a PAN/PVP inner layer and a PBI/POSS outer dense-selective layer for FO and osmotic power generation applications.	2013 [31]
Surface-functionalized PBI flat-sheet membrane	Functionalizing the surface of PBI FO membrane to improve its hydrophilicity and surface charge using *p*-phenylenediamine, ethylene diamine, taurine and poly (acrylamide-*co*-acrylic acid).	2013 [37]
PBI-POSS/PAN HF membranes	Investigating the impact of permeate flux and reverse salt flux on alginate fouling and gypsum scaling of as-spun and annealed PBI–POSS/PAN HF membrane under FO and PRO mode	2014 [42]

Ray-Ran Hand Operated Cutting Press (UK) was used to cut out standard dog-bone specimens. The membrane sample was stretched in tension with a load cell of 10 kN at a strain rate of 1 mm/min, and the response was recorded until failure. Stress–strain curves were plotted from the generated data and were used to determine tensile strength, elastic modulus, and elongation of the membranes. The membrane hydrophilicity was investigated by measuring contact angles at room temperature using Easy Drop Standard contact angle measuring instrument (KRUSS, Germany) equipped with an image processing software. Five contact angles measurements were made for each membrane sample and were averaged to reduce the uncertainties of the measurements. Morphological properties of PBI membranes were studied using Scanning Electron Microscopy (SEM, Quanta 250 FEG, FEI) at 10 kV. Membrane samples were fractured in liquid nitrogen and placed on stainless steel stub using double-coated carbon conductive tape. The samples were sputter coated with Au of 10 nm thickness using a sputtering coater before conducting the SEM analysis. A pressurized dead-end flow cell (Koch, USA) was used to determine the pure water permeability (PWP) of PBI membranes with DI water as feed solution as described elsewhere [36]. The membranes were pre-compacted for 30 mins at 3 bars to achieve stable pure water flux. The water permeability coefficient (A, LMH/bar) was determined using Eq. (1) as follows:

$$A = \frac{J}{\Delta P} \tag{1}$$

where ΔV (L) is the permeate volume, A_m is the effective membrane area, Δt is the permeation time, and ΔP (bar) is the applied pressure difference.

2.4. FO experimental set-up

The bench-scale FO experimental setup used in this study is illustrated in Fig. 1. The membrane cell consisted of two equally structured rectangular flow channels with an effective membrane area of 36 cm^2 (9 cm long, 4 cm wide and 3 mm deep).

Polyester mesh spacers were placed inside the rectangular channels to support the membrane, promote mass transport, and elevate turbulence for minimizing external concentration polarization. Feed and draw solutions were co-currently introduced into the membrane cell at equal flow rates using a two-channel variable-speed peristaltic pump. The active layer of the membrane was oriented towards the draw solution in PRO mode for all the tests performed. The membrane cell was placed inside the water bath at 40 °C to maintain the operating temperature. The draw solution bottle was placed on a hotplate stirrer during the performance test to obtain a well-mixed draw solution at a constant temperature of 40 °C. The feed solution bottle was placed on a Veritas® precision balance with a built-in RS-232 bi-directional communication interface, which was connected to a computer data logging system to record the change in weight of feed tank in real time and determine water flux. The conductivity of both feed and draw solutions was measured using a HQ40d conductivity meter (Hach, Germany) at the start and end of the experiment to determine the reverse salt flux across the FO membrane. The membranes were tested for performance with co-current flow rates of 48 and 141.5 mL/min using 0.63 M NaCl draw solution for a duration of 4 h. The membrane prepared with the best fabrication conditions (demonstrating best performance) was then tested using 2 and 4 M NaCl, and 2 M $MgCl_2$ and KBr draw solutions. The feed and draw solution temperatures were maintained at 23 and 40 °C, respectively for all experiments to mimic the conditions of seawater in Abu Dhabi (UAE). Additionally, the effect of membrane cell orientation on the FO performance was also considered in PRO mode. The membrane cell was horizontally placed inside the water bath in two different orientations. The feed solution was introduced in the top compartment of the FO cell in orientation A; whereas the draw solution was introduced in the top compartment in orientation B. The two orientations are demonstrated schematically in Fig. 2.

The water flux (J_w) across the membrane was obtained by using Eq. (2):

$$J_w = \frac{W_0 - W_e}{\rho \times \Delta t \times A_m} \tag{2}$$

where W_0 and W_e are the feed solution weight (g) before starting and after finishing the performance test, respectively; ρ is water density (g/L), Δt is the duration of performance test (h), and A_m is the effective surface area of the membrane (m^2).

The reverse salt flux (J_s) across the FO membranes was determined using Eq. (3):

$$J_s = \frac{(W_e \times C_{f,e}) - (W_0 \times C_{f,0})}{\rho \times \Delta t \times A_m} \tag{3}$$

where $C_{f,e}$ and $C_{f,0}$ are the salt concentration in the feed solution at the end and start of the performance test, respectively.

The specific reverse salt flux ($SRSF$), which indicates bi-directional diffusion in the FO process was calculated using Eq. (4):

$$SRSF = \frac{J_s}{J_w} \tag{4}$$

The salt rejection ($\%R$) of the FO membranes was calculated using

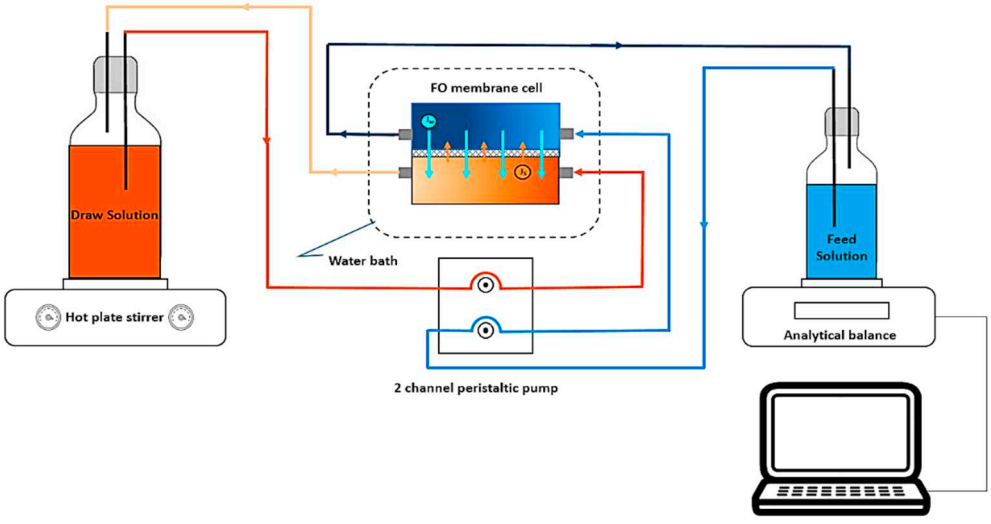

Fig. 1. A schematic diagram of the bench-scale FO experimental setup used for testing the performance of FO membranes.

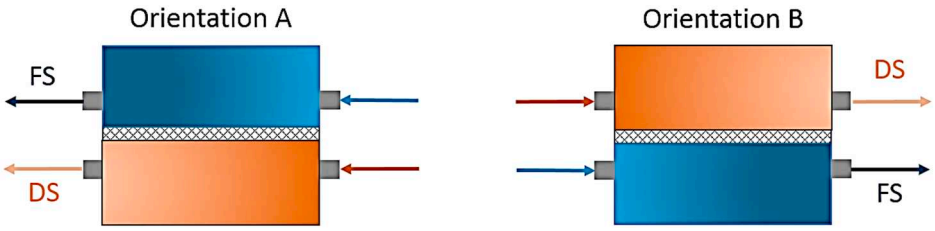

Fig. 2. Two different horizontal FO cell orientations. Orientation A: feed solution (FS) in the top compartment. Orientation B: draw solution (DS) in the top compartment.

Eq. (5):

$$\%R = \left(1 - \frac{J_s/J_w}{(C_{d,0} + C_{d,e})/2}\right) \times 100\% \quad (5)$$

where $C_{d,0}$ and $C_{d,e}$ are the inorganic salt concentrations in the draw solution at the start and end of the performance test, respectively.

The performance of PBI FO flat sheet membrane was enhanced by varying the membrane fabrication conditions. The feed solution was introduced in the top compartment and draw solution in the bottom compartment of the FO cell (orientation A) for all performance tests unless stated otherwise. The parametric study of PBI flat sheet membrane development for FO seawater desalination is divided into three stages as shown in Fig. 3.

2.5. Computational fluid dynamics (CFD) modeling: Impact of concentration gradient across membrane film on water flux and salt rejection

The difference in chemical species concentration leads to diffusion flux, and in laminar and diluted flow (where the concentration of species Y_i is very small) this flux is described according to Fick's law using Eq. (6):

$$J_i = -\rho D_{i,m} \nabla Y_i - D_{i,T} \frac{\nabla T}{T} \quad (6)$$

where $D_{i,m}$ and $D_{i,T}$ are the mass and thermal diffusion coefficients respectively for species i in the multispecies mixture. Turbulence essentially amplifies the diffusion and overwhelms the laminar contribution due to its diffusive nature and $Di_{,m}$ is increased by the ratio between the eddy viscosity and the multiple of turbulence diffusivity by the density (Eq. (7)). The value of the diffusion coefficient has been considered as a fixed and fluid property value, polynomial, and empirical with composition dependent functions [43].

$$D_{i,m} = \frac{\kappa}{\rho \ C_P} \quad (7)$$

where κ is the thermal conductivity, ρ and C_p are the mixture density and specific heat respectively.

These simulations were carried out using the unsteady isothermal Navier-Stokes equations of two species representing the draw and feed solution. The distribution of feed and draw solution was solved only on the draw solution side of the FO cell with an isolated wall bounded domain of 9 cm length and 0.3 cm depth. In the first simulation configuration, a thin layer of the feed solution (DI water) ($\rho = 1000\ kg/m^3$, $C_p = 4182\ J/kg.K$, $\kappa = 0.6\ W/m.K$, dynamic viscosity (M) = 0.001 kg/m.s) was placed beneath the $MgCl_2$ solution ($\rho = 1251\ kg/m^3$, $C_p = 4000\ J/kg.K$, $\kappa = 0.58$ w/m.K, M = 0.0015 kg/m.s) as initial conditions. The computation proceeded at small time step (1.0×10^{-5} s) that satisfies the Currant-Friedrichs Lewy (CFL) stability criteria to accurately capture the flow of temporal evolution. The domain was discretized with a quadrilateral finite volume mesh of 360 × 64 that clustered next to the bottom and top walls to physically resolve the developed boundary layer following direct numerical simulation. In the second simulation/configuration, the feed solution was placed on top of

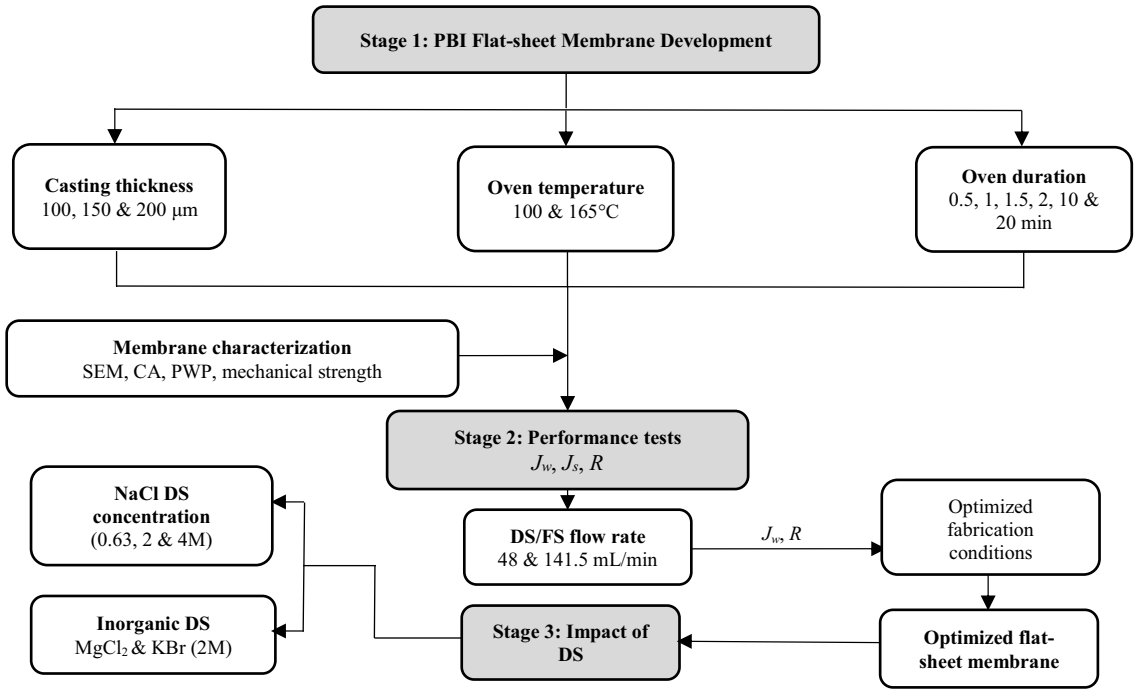

Fig. 3. Parametric study of PBI membrane development for seawater desalination. SEM, CA, PWP, DS, J_w, J_s, and R represent scanning electron microscopy, contact angle, pure water permeability, draw solution, water flux, salt flux and salt rejection, respectively.

the draw solution. The isothermal governing system of equation for the continuity, two-momentum, and species was solved using Fluent Ansys commercial code, which was based on the finite volume method. The differential equations were integrated over the finite volume of a computational cell and over a finite time where a second-order central difference scheme was used in the discretization of the convective and diffusive terms, while the first-order fully implicit scheme is used for time. The semi-implicit solution scheme was adapted for the pressure-velocity coupling in an iterative approach. A tight residual of 1.0×10^{-6} for each of these equations was imposed. A schematic of the model is given in Fig. 11 where the left side shows the boundary conditions and patching of the thin pure species (DI water) of 0.5 mm height.

3. Results and discussions

3.1. Stage 1: Fabrication of PBI FO flat sheet membrane

3.1.1. Effect of oven temperature and heating duration

The 15 wt% PBI film cast on the glass plate was placed in the oven for the formation of a dense active layer. Oven temperature is a critical parameter as it determines the thickness of the dense layer in the FO membrane. Additionally, heat treatment allows stronger adhesion of the casting solution on the support mesh making the PBI membrane stronger. Heat treatment also prevents the membrane from cracking when the film is placed in the water coagulation bath and reduces the pore size of the membrane [23]. Immersing the cast polymer film directly into the water coagulation bath without heat treatment caused the membrane to flake or peel off the mesh. The performance test results using 0.63 M NaCl draw solution at 40 °C, and a flow rate of 48 mL/min are shown in Table 2.

Results showed that the membranes prepared at an oven temperature of 100 °C (Table 2) failed to reject salt resulting in very high SRSF. These membranes were kept in the oven for 10 min and had casting thicknesses of 150 and 200 μm. The dense layer may not have formed at 100 °C, which resulted in high reverse salt flux. Therefore, 100 °C was eliminated, and the performance tests were repeated for membranes using 165 °C keeping all other conditions constant. Oven temperature was chosen as 165 °C because it is the boiling point of polymer solvent. Therefore, it was anticipated that partial evaporation of the solvent in the oven would result in the formation of the membrane's porous support layer below the dense selective layer. The salt rejection of membranes improved when the oven temperature was increased to 165 °C due to dense layer formation (Fig. 4). The membranes with casting thicknesses of 150 and 200 μm at 165 °C oven temperature and 10 min duration in the oven could reject salt by 79.4 and 84.7%, respectively. Therefore, 165 °C was chosen for the PBI membrane preparation.

Following the influence of oven temperature on the membrane preparation process, the effect of membranes' duration in the oven at 165 °C was studied. It was observed that the membrane cast at 150 μm had a *SRSF* of 7.2 g/L when removed from the oven after 10 min but had high *SRSF* of 67.8 g/L when removed after 20 min (Table 2). A duration of 20 min in the oven was too long for membranes cast at 150 μm thickness. As a result, defects were observed on the membrane when it was taken out of the oven (Fig. 4b).

Based on this comparative study, it was decided that the optimal duration of the membrane in the oven will be found at different casting thicknesses by maintaining oven temperature at 165 °C. If the membrane is left in the oven for too long, it may become completely dense with no porous layer, or it can be defective with cracks. Oven duration should be reduced to < 10 min for the formation of a porous layer to enhance membrane water flux and salt rejection. Therefore, oven durations of 0.5, 1, 1.5 and 2 min were chosen to further membrane development.

3.1.2. Effect of membrane thickness

The PBI membranes prepared in this section had casting thickness of 100, 150 and 200 μm, and were placed in the oven for 0.5, 1, 1.5 and 2 min. All the membranes were placed in the oven at 165 °C and immersed in a coagulation bath for 10 min at 23 °C. The performance tests were conducted immediately with a co-current flow rate of 48 mL/min using DI water as feed and 0.63 M NaCl as draw solution at 40 °C. The performance tests results for membranes prepared using different casting thicknesses are shown in Table 3.

As can be observed from Table 3, membranes cast at 100 μm thickness were unable to reject salt, which explains the high *SRSFs* across the defective membranes. The cross-section and morphology of these membranes are shown in Fig. 5. The defects are visible on the membrane surface (Fig. 5a), and there was no formation of dense layer (Fig. 5b) which has resulted in no salt rejection. Since similar observations have been made for all membranes with a casting thickness of 100 μm, it may be concluded that 100 μm was not thick enough for the formation of a dense selective layer. Although thin selective layers are desirable for improving water flux, they can significantly decrease salt rejection. A desirable FO membrane should have a highly selective active layer for enhancing salt rejection and very hydrophilic and porous support with low tortuosity to minimize ICP [44]. Therefore, it could be concluded that improving the hydrophilicity of the membrane surface is much better than decreasing the membrane thickness as it allows selective improvement in water flux without increasing the reverse salt flux [45].

Besides the membranes with a casting thickness of 100 μm, all other membranes at conditions listed in Table 3 were characterized and tested for performance at a higher flow rate of 141.5 mL/min using 0.63 M NaCl draw solution.

3.1.3. Membrane characterization

3.1.3.1. Mechanical properties and contact angle measurements. The membrane characterization data is provided in Table 4. It was found that the membrane elongation increased at higher oven duration and casting thickness, but tensile strength decreased with increasing casting thickness. The highest elongation at break was 73.2%, which was obtained for a membrane with a casting thickness of 200 μm and oven duration of 2 min. The highest tensile strength obtained was 79.7 MPa for a membrane with a casting thickness of 150 μm and oven duration of 2 min. It may be deduced that longer duration of heat treatment and grater casting thickness made the membranes more ductile and reduced their tensile strength do to change in membrane morphology. PBI

Table 2
Performance test results for choosing the optimal oven temperature. All membranes were placed in coagulation bath for 10 min at coagulant temperature of 23 °C. Performance tests were run at a flow rate of 48 mL/min for 4 h with 0.63 M NaCl draw solution.

Oven temperature (°C)	Oven time (min)	Casting thickness (μm)	J_w (LMH)	J_s (GMH)	*SRSF* (g/L)	*R* (%)
100	10	150	0.03 ± 0.02	15.14 ± 1.99	504.7	–
100	10	200	0.04 ± 0.01	14.29 ± 1.89	357.3	–
165	10	150	0.10 ± 0.02	0.72 ± 0.11	7.2	79.4 ± 4.9
165	10	200	0.13 ± 0.02	0.76 ± 0.34	5.9	84.7 ± 5.5
165	20	150	0.06 ± 0.00	4.07 ± 0.00	67.8	–
165	20	200	0.14 ± 0.02	0.09 ± 0.02	0.6	98.1 ± 0.1

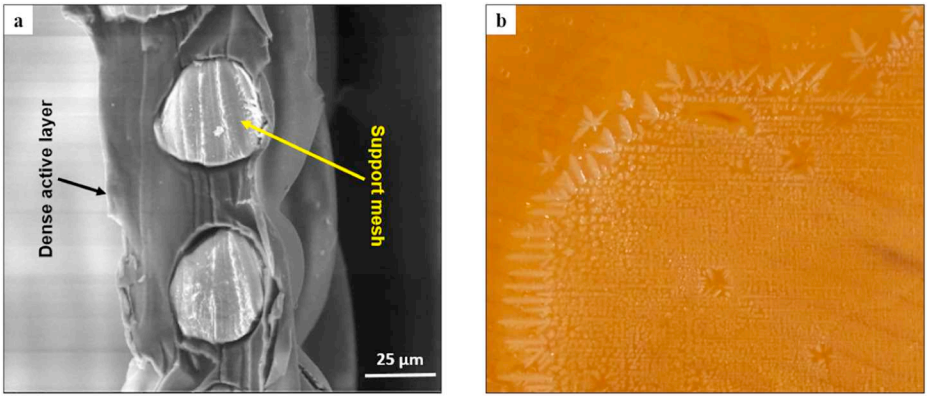

Fig. 4. (a) SEM cross-sectional image of PBI membrane prepared using 15 wt% PBI casting solution, 200 µm casting thickness, duration of 20 min in the oven at 165 °C and placed in coagulation bath for 10 min at 23 °C. (b) A damaged membrane with a casting thickness of 150 µm, placed in the oven for 20 min at 165 °C.

Table 3
Performance test results for membranes prepared using 15 wt% PBI dope. All membranes were placed in an oven at 165 °C, and in coagulation bath for 10 min at 23 °C. Performance tests were run at a flow rate of 48 mL/min for 4 h with 0.63 M NaCl draw solution.

Dope concentration: 15 wt% PBI					
Casting thickness (µm)	**Oven time (min)**	J_w **(LMH)**	J_s **(GMH)**	***SRSF*** **(g/L)**	***R*** **(%)**
100	0.5	0.3	15.01	50.1	–
100	1	0.11	16.84	153.1	–
100	1.5	0.51	52.43	102.8	–
150	1.5	1.68	7.82	4.7	87.2
150	2	0.12	1.67	13.9	61.3
200	1.5	0.69	3.04	4.4	87.8
200	2	0.1	0.31	3.1	90.9

membrane cast using 15 wt% PBI dope with a casting thickness of 150 µm and oven duration of 1.5 min was found to be the stiffest with an elastic modulus of 375.2 MPa.

The water contact angle measurements of selected PBI flat sheet membranes at different fabrication conditions were measured (Table 4). It was found that the PBI membranes retained their hydrophilicity at all fabrication conditions. The hydrophilic nature of the membranes ensures their wettability. The least hydrophilic membrane with a contact angle of 77.3° was the one cast at 200 µm thickness and left in the oven for 2 min at 165 °C. The most hydrophilic membrane with a contact angle of 48.2° was the one cast at 150 µm thickness, which was left in the oven for 1.5 min at 165 °C. The contact angles obtained in this study were found to be close to the previously reported value of around 75° for virgin PBI membranes [37]. Membranes became less hydrophilic when they were heated in the oven for longer and the membrane casting thickness was increased from 150 to 200 µm for same fabrication conditions (Table 4).

Table 4
Characterization of 15 wt% PBI FO membrane.

Casting thickness (µm)	Oven duration (min)	Tensile strength (MPa)	Elongation (%)	Elastic modulus (MPa)	Contact angle (°)
150	1.5	77.5	36.5	375.2 ± 6.9	48.2 ± 2.2
150	2	79.7	68.2	158.5 ± 8.6	66.7 ± 1.4
200	1.5	44.1	53.6	90.4 ± 4.4	74.5 ± 3.7
200	2	35.7	73.2	48.5 ± 0.9	77.3 ± 1.5

3.1.3.2. Membrane morphology. The SEM images of the PBI membrane cross-section prepared using 15 wt% PBI dope are shown in Fig. 6. Spongy support layer was observed for membranes with oven duration of 1.5 min and casting thickness of 150 µm (Fig. 6a) and 200 µm (Fig. 6c). Whereas, dense support layer was observed for membranes that were heat cured for 2 min (Figs. 6b and d). Based on the observed membrane morphology, it can be deduced that a longer duration of heat treatment forms denser membranes.

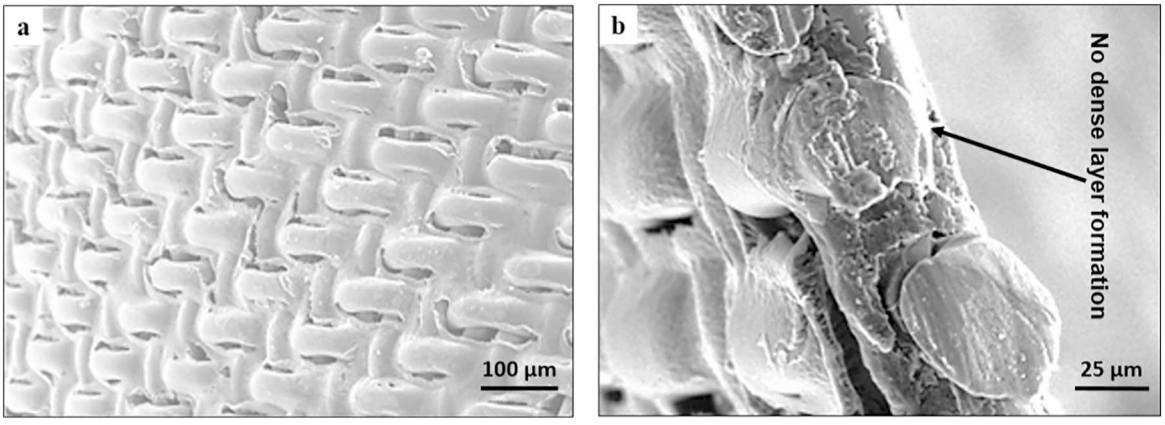

Fig. 5. SEM images of PBI membrane prepared using 15 wt% PBI casting solution, 100 µm casting thickness, duration of 30 s in oven at 165 °C and placed in coagulation bath for 10 min at 23 °C (a) support layer (b) cross section of membrane.

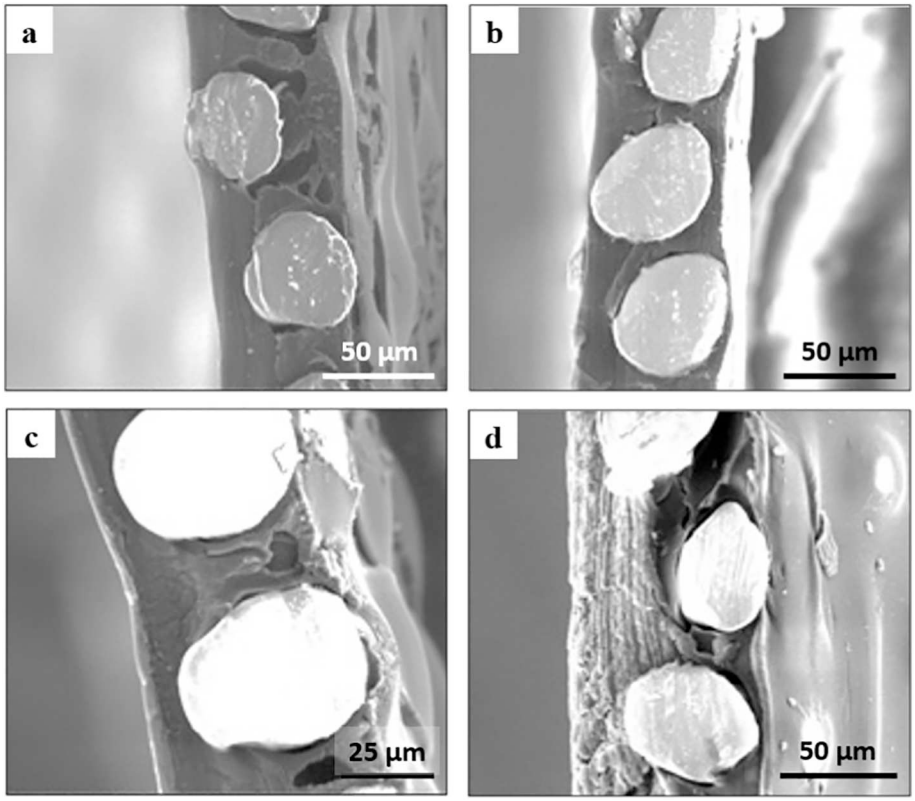

Fig. 6. Cross-sectional SEM images of 15 wt% PBI membranes. The casting thickness and oven duration of the membranes are: a) 150 µm, 1.5 min b) 150 µm, 2 min c) 200 µm, 1.5 min d) 200 µm, 2 min. Membranes are placed in oven at 165 °C and in water coagulation bath for 10 min at 23 °C.

3.2. Stage 2: Performance tests at the different draw and feed solution flow rates

The performance test results for membranes cast using 15 wt% PBI are presented in Fig. 7. Optimal performing membrane was chosen to be the one demonstrating good water flux and high salt rejection overall. The membranes that were heat treated for 2 min demonstrated higher salt rejection and lower water flux due to the formation of a very dense and thick active layer. Based on the performance tests, the best performing membrane was chosen to be the one prepared using 15 wt% PBI dope with a casting thickness of 150 µm, heated in the oven for 1.5 min at 165 °C and followed by immersion in water coagulation bath for 10 min at 23 °C. The comparatively less dense structure of the optimal membrane allowed it to achieve the highest water flux and salt rejection of 2.0 LMH and 95.57%, respectively at a flow rate of 141.5 mL/min. The pure water permeability of the optimized membrane was found to be 1.6 ± 0.1 LMH/bar.

3.3. Stage 3: Impact of draw solution

The membrane prepared at the optimized conditions (15 wt% PBI dope, 150 µm casting thickness, 1.5 min in the oven at 165 °C, 10 min in coagulation bath at 23 °C) was then tested for performance at higher NaCl draw solution concentrations and with different inorganic draw solutions. Fig. 8 represents the water flux demonstrated by the optimized PBI membrane using DI water as the feed solution and NaCl draw solution at concentrations of 0.63, 2 and 4 M under PRO orientation. The water flux across the PBI flat sheet membrane increased with increasing NaCl draw solution concentration because of an increase in the osmotic pressure of draw solution, which is the main driving force in FO processes. The PBI membrane demonstrated water fluxes of 4.7 LMH and 2.0 LMH using 4 M and 0.63 M NaCl as DS, respectively.

In addition to NaCl, KBr and $MgCl_2$ were used as draw solutions at a concentration of 2 M. The performance of the optimal membrane was tested at a flow rate of 141.5 mL/min using these draw solutions at 40 °C. $MgCl_2$ solution yielded the highest water flux (4.2 LMH), and KBr solution gave the lowest water flux (2.3 LMH) as can be seen in Fig. 9. This is because $MgCl_2$ has the highest and KBr has the lowest osmotic pressure. Moreover, highest salt rejection was obtained using $MgCl_2$ draw solution (97.4%), and the lowest was obtained using KBr draw solution (96%). Salt rejection was highest for $MgCl_2$ because it has the largest ion size; thereby, reducing reverse salt flux. Whereas, the ion size for KBr is the smallest among the three draw solutions used.

3.4. Effect of FO membrane cell horizontal orientations

Since the membrane cell was aligned horizontally, introducing the feed solution into the top or bottom compartment may influence the water and reverse salt flux across the membrane. Experiments using the PBI membrane were conducted in both orientation A and B (Fig. 2) to study the effect of cell orientation of membrane performance. The temperature of feed and draw solutions were maintained at 23 and 40 °C respectively and were circulated co-currently at a flow rate of 141.5 mL/min. The performance results (Fig. 10) showed that both the water flux and salt rejection improved when the draw solution was allowed to flow in the top compartment of the membrane cell (orientation B) instead of the feed solution. The water flux and salt rejection with 0.63 M NaCl draw solution increased from 2.0 to 5.8 LMH and 95.6 to 96.9%, respectively when the FO cell orientation was changed from A to B. Similarly, the water flux and salt rejection with 2 M $MgCl_2$ draw solution increased from 4.2 to 21.3 LMH and 97.4 to 98.8%, respectively when the FO cell orientation was changed from A to B.

There was a 4 and 6 folds increase approximately in the water flux using NaCl and $MgCl_2$ draw solutions, respectively. The salt rejection for both NaCl and $MgCl_2$ draw solutions was higher in orientation B

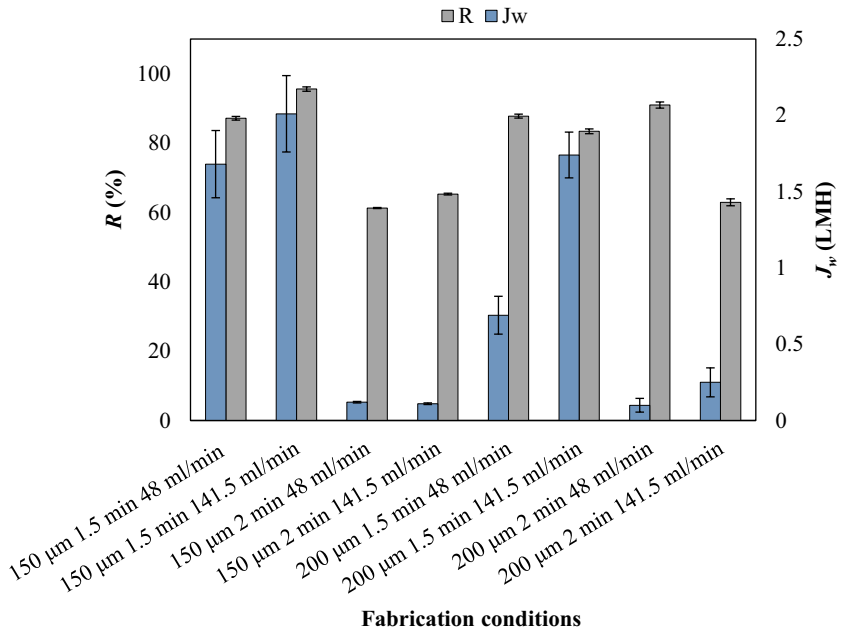

Fig. 7. Performance of PBI membranes cast with 15 wt% PBI dope at casting thickness of 150 and 200 µm, duration of 1.5 and 2 min in the oven. Performance tests were run using 0.63 M NaCl draw solution at 40 °C and flow rates of 48 and 141.5 mL/min.

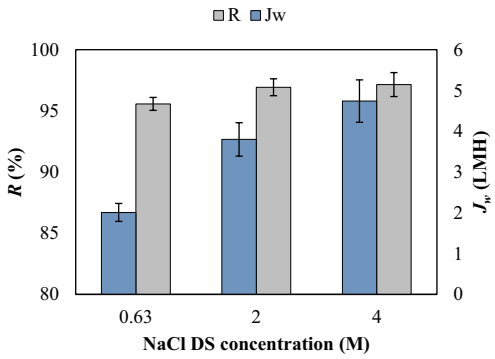

Fig. 8. Performance of optimal membrane tested using different NaCl draw solution concentration at 40 °C, DI water feed at 23 °C and flow rate of 141.5 mL/min.

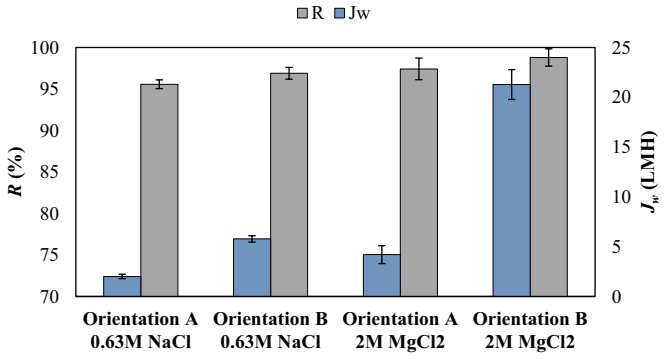

Fig. 10. Performance results of PBI membrane in cell orientation A and B using 0.63 M NaCl and 2 M $MgCl_2$ draw solutions at 40 °C, and DI water feed at 23 °C at a flow rate of 141.5 mL/min.

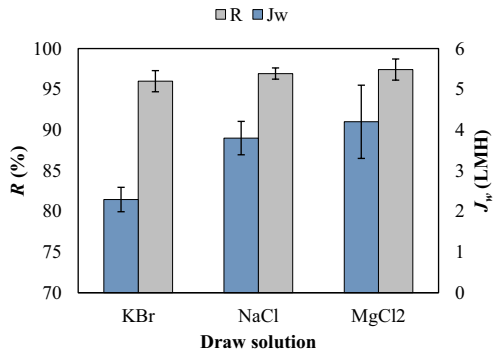

Fig. 9. Performance of optimal membrane tested using 2 M draw solution at 40 °C, DI water feed at 23 °C and flow rate of 141.5 mL/min.

than A. The improved flow dynamics within the membrane cell could have possibly resulted in higher water flux and salt rejection. Therefore, membrane cell orientation is an essential operational parameter that should be taken into consideration as it may significantly affect the efficiency and performance of the FO process. For this reason, computational fluid dynamics (CFD) modeling was used to further investigate the effect of concentration gradient across membrane surface on water flux and salt rejection at different cell orientations.

3.5. Computational fluid dynamics (CFD) modeling: Impact of concentration gradient across membrane film on water flux and salt rejection at different cell orientations

Fig. 11 depicts the computational domain setup and results in terms of color contours plots of mass fraction distribution of the pure fluid/flux over time for the two FO cell configurations. Fig. 11a represents the initial intense and chaotic diffusion of the feed solution (less dense) in the first second due to gravity when the draw solution (denser) was positioned at the top of the membrane. However, as shown in Fig. 11b, the diffusion is almost unnoticeable in the first second when the draw solution was positioned at the bottom of the membrane. Due to the initiation of concentration polarization, the FO performance is hindered in the second scenario.

In addition, Figs. 12 and 13 depict the vertical line plots of the captured contours (Fig. 11) for a better quantitative comparison. When

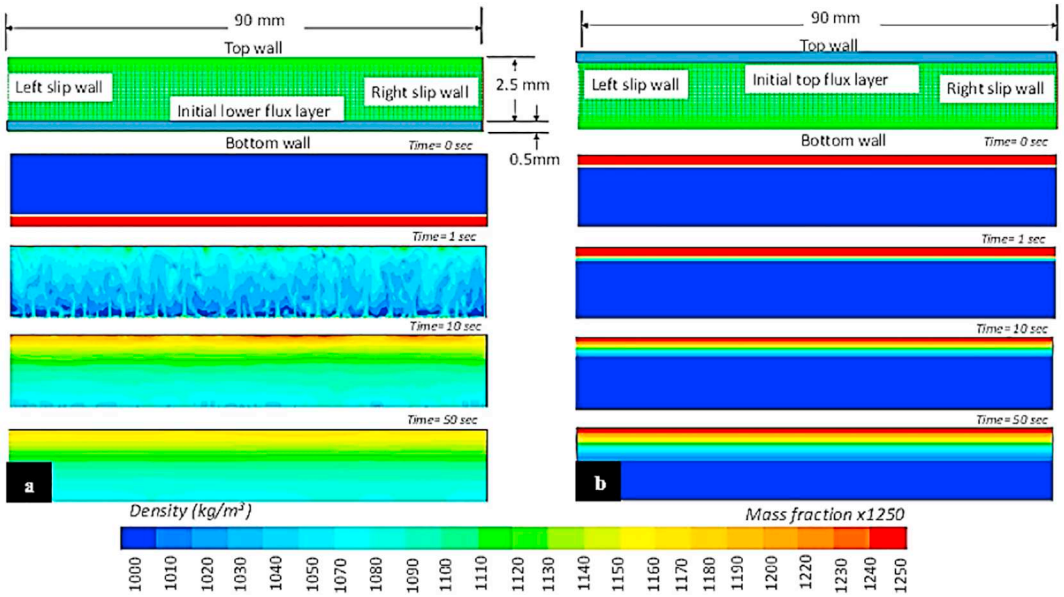

Fig. 11. Computational domain representing only the draw solution side of the FO cell and when draw solution is located on the (a) top and (b) bottom of the membrane. It is layered with a small flux adjacent to the membrane as an initial condition. The density or mass fraction contours represents the diffusion in both cell orientations.

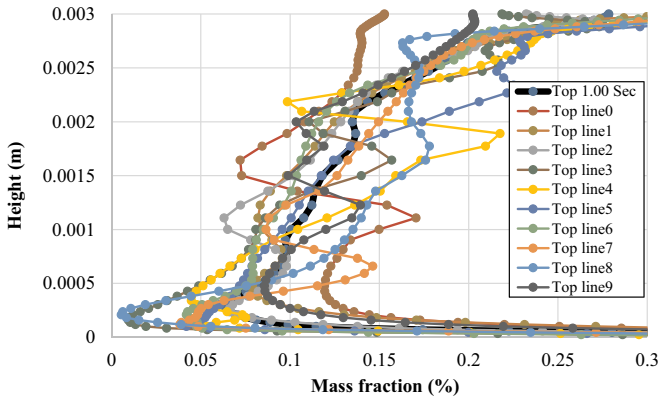

(a)

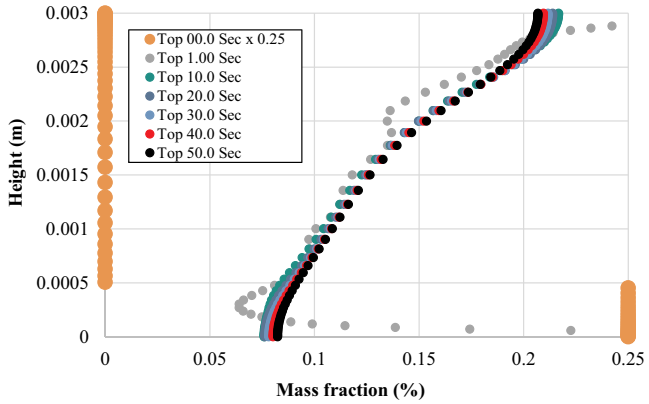

(b)

Fig. 12. (a) Vertical line plots taken 1 cm apart in the 9 cm domain representing the flux fraction after 1 s, and their average (black line) when the draw solution side was placed on top. (b) Average of 9 lines at six different times starting at $t = 0$, then 1, 10, 20, 30, 40 and 50 s.

denser draw solution was located at the top of the membrane; less dense feed solution would diffuse across the membrane from the feed side to the draw side. Once the feed solution diffuses to the draw solution side, it will move upward towards the cell owing to its lower density; therefore, getting replaced by the denser draw solution on the membrane surface, which in turn mitigates concentration polarization (Fig. 12). On the contrary, the diffusion rate was observed to be very slow in the first second when the draw solution was located at the

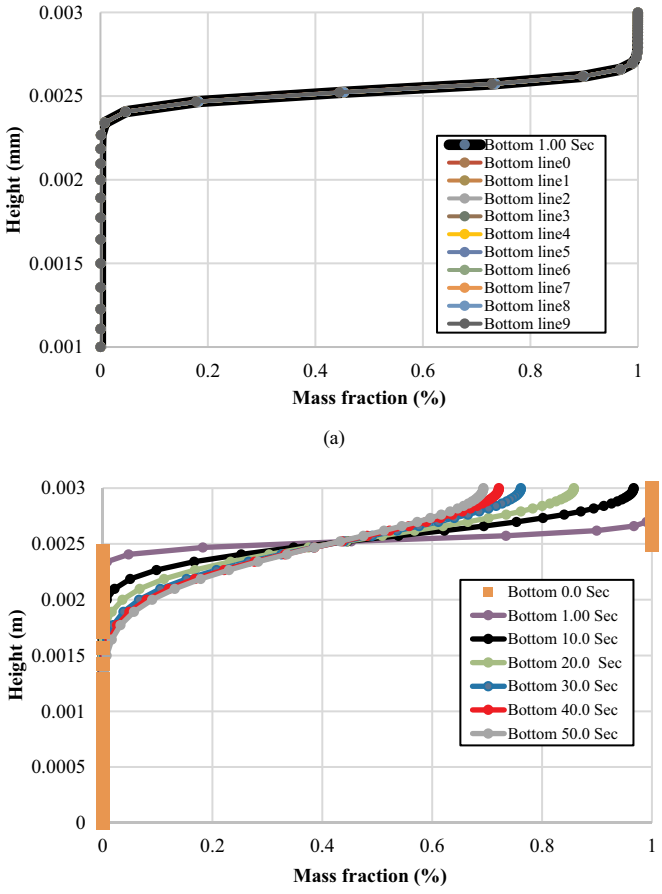

Fig. 13. (a) Vertical line plots taken 1 cm apart in the 9 cm domain representing the flux fraction after 1 s, and their average (black line) when the draw solution side was placed at the bottom (note that all lines co-exist). (b) Average of 9 lines at six different times starting at t = 0, then 1, 10, 20, 30, 40 and 50 s.

bottom of the membrane (Fig. 13). As a result, the feed solution started to accumulate near the membrane surface at the top, while gravity effect would act in the opposite direction of the mass diffusion. Nevertheless, the diffusion would eventually overcome gravity forces but at a much lower rate compared to that achieved when the draw solution was positioned on the top.

To sum it up, gravity-induced diffusion was mentioned in a few recent articles; however, progress in computational fluid dynamics can unravel the role of gravity on fluid mixing [46,47]. Concentration polarization is one of the drawbacks in FO and external concentration polarization can be mitigated via turbulence to enhance the process performance. In general, it is believed that gravity has a negligible effect on molecular/ionic diffusion. The ions of a substance, in the case of NaCl, naturally create homogeneity as they dissolve in water, but the effect of gravity creates a downward force on these ions that may reduce the diffusion rate. Although studies on diffusion showed that this force is negligible, in the case of two fluids with different specific weight with a small cross-flow velocity, this effect cannot be ignored. Considering the case of two fluids with different densities, with the denser fluid (draw solution) on top of a less dense fluid (feed solution), gravity would trigger flow instability. The fluid goes into transient state motion that initially resembles a chaotic behavior before it reaches a stable state. These results have been revealed via numerical simulation of the high fidelity unsteady Navier-Stokes flow over the draw solution side from the membrane of FO setup in line with the DCMD simulation [46,47]. It clearly showed the advantage of placing the draw solution on the upper channel side of the membrane, which prevents the increasing concentration polarization that occurs when the denser draw solution side is placed below the membrane. It could be summarized that the diffusion rate is a critical factor in a continuous system with low cross-flow velocity like the one used in this study, where the process is driven by the incoming flow of the draw solution which resides in the channel during its transfer time. The transfer time is equivalent to the channel length divided by the cross-flow velocity. Therefore, positioning draw solution at the bottom requires a higher flow speed to overcome the lower attained diffusion rate.

3.6. Comparison of PBI membranes performance used in FO processes

Table 5 presents the performance of PBI FO membranes reported in this work and other studies. The water flux obtained in this study is close to those reported in the literature for the flat sheet membrane. The functionalized hollow fiber membranes reported in other studies; however, have a higher water flux which could be attributed to their larger membrane surface area and higher cross flow velocity than that used in this work. The reported membrane permeate fluxes are not high enough to make FO process commercially feasible. PBI membranes still need further modification before they can be used for commercial applications.

4. Conclusions

Asymmetric PBI flat sheet membranes were prepared via immersion phase inversion technique for seawater desalination applications in high temperature and high salinity regions. Several membrane fabrication conditions were varied. These included membrane casting

Table 5
Comparison of PBI FO membrane performance.

Membrane	Material	FO performance (PRO mode)		Performance testing conditions				Reference
		J_w (LMH)	R (%)	Feed solution	Draw solution	Temperature (°C)	Cross flow velocity (flow rate)	
Asymmetric flat sheet membrane (Orientation A)	PBI (15 wt%)	3.80	96.93	DI	2 M NaCl	40	1.97 cm/s (141.5 ml/min)	This work
Asymmetric flat sheet membrane (Orientation B)	PBI (15 wt%)	21.28	98.80	DI	2 M $MgCl_2$	40	1.97 cm/s (141.5 ml/min)	This work
Asymmetric flat sheet membrane	PBI (26 wt%)	2.0	NR	0.1 M NaCl	2 M NH_4HCO_3	RT	65 ml/min	[37]
Asymmetric HFM	PBI	3.84	97	DI	2 M NaCl	RT	9.2 cm/s (lumen) 0.6 cm/s (shell)	[33]
Asymmetric HFM	PBI	9.02	99	DI	2 M $MgCl_2$	RT	9.2 cm/s (lumen) 0.6 cm/s (shell)	[33]
Asymmetric HFM	p-xylylene dichloride cross-linked PBI	36.5	NR	DI	5 M $MgCl_2$	RT	8 cm/s	[38]
Dual Layer HFM	Annealed PBI- POSS/ PAN	17.4	NR	DI	1.6 M NaCl	RT	23 cm/s	[42]

thickness, oven temperature and duration. Also, the impact of FO process operational parameters such as feed and draw solutions flow rates, draw solution type and concentration, and membrane cell orientation (i.e., A and B) was investigated on the performance of the PBI membrane. Results showed 2 M $MgCl_2$ reported the highest water flux and a salt rejection of 4.2 LMH and 97.4% when compared to 2 M NaCl and KBr draw solutions (i.e., 3.8 LMH and 96.9%, and 2.3 LMH and 96%, respectively). The performance results showed that both the water flux and salt rejection improved when the draw solution was allowed to flow in the top compartment of the membrane cell (orientation B) instead of the feed solution. The water flux and salt rejection with 0.63 M NaCl draw solution increased from 2.0 to 5.8 LMH and 95.6 to 96.9%, respectively when the FO cell orientation was changed from A to B. Similarly, the water flux and salt rejection with 2 M $MgCl_2$ draw solution increased from 4.2 to 21.3 LMH and 97.4 to 98.8%, respectively when the FO cell orientation was changed from A to B. CFD modeling results demonstrated that solution density, gravity and diffusion rate affected FO performance at low cross-flow velocity. Further modification of PBI membranes and more studies need to be conducted to enhance the performance of PBI membranes for FO processes.

Acknowledgments

Authors would like to thank Trevi Systems, Inc. (USA), Masdar and Masdar Institute of Science and Technology (as part of Khalifa University of Science and Technology, Abu Dhabi - UAE) for supporting this research (Grant. No. EX2014-000040).

References

[1] L. Chekli, S. Phuntsho, H.K. Shon, S. Vigneswaran, J. Kandasamy, A. Chanan, A review of draw solutes in forward osmosis process and their use in modern applications, Desalin. Water Treat. 43 (2012) 167–184.
[2] R.E. Kravath, J.A. Davis, Desalination of sea water by direct osmosis, Desalination 16 (1975) 151–155.
[3] G.W. Batchelder, Process for the demineralization of water, in, Google Patents, 1965.
[4] J.R. McCutcheon, R.L. McGinnis, M. Elimelech, A novel ammonia—carbon dioxide forward (direct) osmosis desalination process, Desalination 174 (2005) 1–11.
[5] S. Zhao, L. Zou, C.Y. Tang, D. Mulcahy, Recent developments in forward osmosis: opportunities and challenges, J. Membr. Sci. 396 (2012) 1–21.
[6] S. Loeb, Energy production at the Dead Sea by pressure-retarded osmosis: challenge or chimera? Desalination 120 (1998) 247–262.
[7] R.S. Norman, Water salination: a source of energy, Science 186 (1974) 350–352.
[8] A. Achilli, T.Y. Cath, E.A. Marchand, A.E. Childress, The forward osmosis membrane bioreactor: a low fouling alternative to MBR processes, Desalination 239 (2009) 10–21.
[9] B.D. Coday, P. Xu, E.G. Beaudry, J. Herron, K. Lampi, N.T. Hancock, T.Y. Cath, The sweet spot of forward osmosis: treatment of produced water, drilling wastewater, and other complex and difficult liquid streams, Desalination 333 (2014) 23–35.
[10] D.D. Kaombe, M.-B. Hägg, Forward osmosis for the dewatering of pyrolysis oil aqueous phase, Sep. Purif. Technol. 138 (2014) 92–97.
[11] K.L. Hickenbottom, N.T. Hancock, N.R. Hutchings, E.W. Appleton, E.G. Beaudry, P. Xu, T.Y. Cath, Forward osmosis treatment of drilling mud and fracturing wastewater from oil and gas operations, Desalination 312 (2013) 60–66.
[12] P.H. Duong, T.-S. Chung, Application of thin film composite membranes with forward osmosis technology for the separation of emulsified oil–water, J. Membr. Sci. 452 (2014) 117–126.
[13] S. Zhang, K.Y. Wang, T.-S. Chung, H. Chen, Y.C. Jean, G. Amy, Well-constructed cellulose acetate membranes for forward osmosis: minimized internal concentration polarization with an ultra-thin selective layer, J. Membr. Sci. 360 (2010) 522–535.
[14] N. Akther, A. Sodiq, A. Giwa, S. Daer, H. Arafat, S. Hasan, Recent advancements in forward osmosis desalination: a review, Chem. Eng. J. 281 (2015) 502–522.
[15] C.R. Martinetti, A.E. Childress, T.Y. Cath, High recovery of concentrated RO brines using forward osmosis and membrane distillation, J. Membr. Sci. 331 (2009) 31–39.
[16] T.Y. Cath, A.E. Childress, M. Elimelech, Forward osmosis: principles, applications, and recent developments, J. Membr. Sci. 281 (2006) 70–87.
[17] D.L. Shaffer, J.R. Werber, H. Jaramillo, S. Lin, M. Elimelech, Forward osmosis: where are we now? Desalination 356 (2015) 271–284.
[18] Q. Ge, M. Ling, T.-S. Chung, Draw solutions for forward osmosis processes: developments, challenges, and prospects for the future, J. Membr. Sci. 442 (2013) 225–237.
[19] R.K. McGovern, J.H. Lienhard, V, on the potential of forward osmosis to energetically outperform reverse osmosis desalination, J. Membr. Sci. 469 (2014) 245–250.
[20] E.W. Tow, R.K. McGovern, Raising forward osmosis brine concentration efficiency

through flow rate optimization, Desalination 366 (2015) 71–79.
[21] W. Tang, H.Y. Ng, Concentration of brine by forward osmosis: performance and influence of membrane structure, Desalination 224 (2008) 143–153.
[22] W.M. Thomas, Copolymers of acrylonitrile, in, Google Patents, 1959.
[23] L. Sawyer, R. Jones, Observations on the structure of first generation polybenzimidazole reverse osmosis membranes, J. Membr. Sci. 20 (1984) 147–166.
[24] K. Kreuer, A. Fuchs, M. Ise, M. Spaeth, J. Maier, Imidazole and pyrazole-based proton conducting polymers and liquids, Electrochim. Acta 43 (1998) 1281–1288.
[25] K.Y. Wang, T.S. Chung, Polybenzimidazole nanofiltration hollow fiber for cephalexin separation, AICHE J. 52 (2006) 1363–1377.
[26] P. Staiti, F. Lufrano, A. Arico, E. Passalacqua, V. Antonucci, Sulfonated polybenzimidazole membranes—preparation and physico-chemical characterization, J. Membr. Sci. 188 (2001) 71–78.
[27] L. Xiao, H. Zhang, E. Scanlon, L. Ramanathan, E.-W. Choe, D. Rogers, T. Apple, B.C. Benicewicz, High-temperature polybenzimidazole fuel cell membranes via a sol-gel process, Chem. Mater. 17 (2005) 5328–5333.
[28] B. Xing, O. Savadogo, Hydrogen/oxygen polymer electrolyte membrane fuel cells (PEMFCs) based on alkaline-doped polybenzimidazole (PBI), Electrochem. Commun. 2 (2000) 697–702.
[29] S. Kumbharkar, Y. Liu, K. Li, High performance polybenzimidazole based asymmetric hollow fibre membranes for H 2/CO 2 separation, J. Membr. Sci. 375 (2011) 231–240.
[30] W.-P. Zhu, S.-P. Sun, J. Gao, F.-J. Fu, T.-S. Chung, Dual-layer polybenzimidazole/polyethersulfone (PBI/PES) nanofiltration (NF) hollow fiber membranes for heavy metals removal from wastewater, J. Membr. Sci. 456 (2014) 117–127.
[31] F.-J. Fu, S. Zhang, S.-P. Sun, K.-Y. Wang, T.-S. Chung, POSS-containing delamination-free dual-layer hollow fiber membranes for forward osmosis and osmotic power generation, J. Membr. Sci. 443 (2013) 144–155.
[32] L.P. Raman, M. Cheryna, N. Rajagopalan, Consider nanofiltration for membrane separations, Chemical Engineering Progress, 1994, p. 90 (United States).
[33] K.Y. Wang, T.-S. Chung, J.-J. Qin, Polybenzimidazole (PBI) nanofiltration hollow fiber membranes applied in forward osmosis process, J. Membr. Sci. 300 (2007) 6–12.
[34] J. Lv, K.Y. Wang, T.-S. Chung, Investigation of amphoteric polybenzimidazole (PBI) nanofiltration hollow fiber membrane for both cation and anions removal, J. Membr. Sci. 310 (2008) 557–566.
[35] K.Y. Wang, Y. Xiao, T.-S. Chung, Chemically modified polybenzimidazole nanofiltration membrane for the separation of electrolytes and cephalexin, Chem. Eng. Sci. 61 (2006) 5807–5817.
[36] R. Hausman, B. Digman, I.C. Escobar, M. Coleman, T.-S. Chung, Functionalization of polybenzimidizole membranes to impart negative charge and hydrophilicity, J. Membr. Sci. 363 (2010) 195–203.
[37] M.F. Flanagan, I.C. Escobar, Novel charged and hydrophilized polybenzimidazole (PBI) membranes for forward osmosis, J. Membr. Sci. 434 (2013) 85–92.
[38] K.Y. Wang, Q. Yang, T.-S. Chung, R. Rajagopalan, Enhanced forward osmosis from chemically modified polybenzimidazole (PBI) nanofiltration hollow fiber membranes with a thin wall, Chem. Eng. Sci. 64 (2009) 1577–1584.
[39] Q. Yang, K.Y. Wang, T.-S. Chung, Dual-layer hollow fibers with enhanced flux as novel forward osmosis membranes for water production, Environ. Sci. Technol. 43 (2009) 2800–2805.
[40] Q. Yang, K.Y. Wang, T.-S. Chung, A novel dual-layer forward osmosis membrane for protein enrichment and concentration, Sep. Purif. Technol. 69 (2009) 269–274.
[41] J. Su, Q. Yang, J.F. Teo, T.-S. Chung, Cellulose acetate nanofiltration hollow fiber membranes for forward osmosis processes, J. Membr. Sci. 355 (2010) 36–44.
[42] S.C. Chen, X.Z. Fu, T.-S. Chung, Fouling behaviors of polybenzimidazole (PBI)–polyhedral oligomeric silsesquioxane (POSS)/polyacrylonitrile (PAN) hollow fiber membranes for engineering osmosis processes, Desalination 335 (2014) 17–26.
[43] K.K.-y. Kuo, Principles of Combustion, John Wiley and Sons Ltd, New York, United States, 1987.
[44] S. Phuntsho, S. Sahebi, T. Majeed, F. Lotfi, J.E. Kim, H.K. Shon, Assessing the major factors affecting the performances of forward osmosis and its implications on the desalination process, Chem. Eng. J. 231 (2013) 484–496.
[45] Y. Yu, S. Seo, I.-C. Kim, S. Lee, Nanoporous polyethersulfone (PES) membrane with enhanced flux applied in forward osmosis process, J. Membr. Sci. 375 (2011) 63–68.
[46] I. Janajreh, K. El Kadi, R. Hashaikeh, R. Ahmed, Numerical investigation of air gap membrane distillation (AGMD): seeking optimal performance, Desalination 424 (2017) 122–130.
[47] I. Janajreh, D. Suwwan, R. Hashaikeh, Assessment of direct contact membrane distillation under different configurations, velocities and membrane properties, Appl. Energy 185 (2017) 2058–2073.